Role of surface spins on magnetization of Cr_2O_3 coated γ-Fe_2O_3 nanoparticles

K. Nadeem[a,*], M. Kamran[a], A. Javed[a], F. Zeb[a], S.S. Hussain[a], M. Mumtaz[a], H. Krenn[b], D.V. Szabo[c,d], U. Brossmann[e], Xiaoke Mu[f]

[a] *Nanoscience and Technology Laboratory, International Islamic University, Islamabad, 44000, Pakistan*
[b] *Institute of Physics, Karl-Franzens University, Universitätsplatz 5, A-8010, Graz, Austria*
[c] *Institute for Applied Materials, Karlsruhe Institute of Technology (KIT), D-76344, Eggenstein-Leopoldshafen, Germany*
[d] *Karlsruhe Nano Micro Facility (KNMF), Karlsruhe Institute of Technology (KIT), D-76344, Eggenstein-Leopoldshafen, Germany*
[e] *Institute of Materials Physics, University of Technology Graz, A-8010, Graz, Austria*
[f] *Institute of Nanotechnology, Karlsruhe Institute of Technology (KIT), D-76344, Eggenstein-Leopoldshafen, Germany*

A R T I C L E I N F O

Keywords:
Maghemite
Cr_2O_3 coating
Nanoparticles
Spin-glass
Magnetic properties

A B S T R A C T

Effect of surface spins in chromium oxide (Cr_2O_3) coated maghemite (γ-Fe_2O_3) nanoparticles (13 nm) as prepared by microwave plasma technique have been studied in detail. The temperature dependent zero field cooled/field cooled (ZFC/FC) measurements revealed the blocking temperature at $T_B = 75$ K. Simulated ZFC/FC curves exhibited large value of effective anisotropy of Cr_2O_3 coated γ-Fe_2O_3 nanoparticles as compared to bulk γ-Fe_2O_3 but less than bare γ-Fe_2O_3 nanoparticles. Bloch's law was fitted on M_S-T data and revealed the values of Bloch's constant $B = 3.523 \times 10^{-4}\,K^{-b}$ and Bloch's exponent $b = 1.10$. The higher value of B than in bulk is due to weaker exchange coupling J ($B \sim 1/J$) on the surface of nanoparticle due to disorder surface spins, while lower value of b is due to no spin wave excitation in presence of large energy band gap at nanoscale. Kneller's law fit on H_C-T data deviated in all temperature range which is due to strong surface anisotropy, core-shell interactions and superparamagnetism. Interparticle interactions and spin glass behavior were investigated by using different physical laws for f-dependent ac susceptibility and they confirmed the presence of spin glass behavior which is due to disordered frozen surface spins and random interparticle interactions.

1. Introduction

Surface effects arise in nanoparticles due to high surface to volume ratio which can directly influence the magnetization reversal and relaxation of magnetic nanoparticles [1]. Spin disorder, surface anisotropy and weak exchange coupling near and at the surface modify the structural, electronic and magnetic properties of ferrite nanoparticles. The surface anisotropy, high field irreversibility and high coercivity, non saturation magnetization at low temperature provide clear evidence of spin glass behavior at low temperature [2–6].

Maghemite (γ Fe_2O_3) nanoparticles are promising candidate for different applications such as in biomedical therapy and diagnostic, ferro fluids, magnetic tunneling barrier for spin filter devices and magnetic data recording [7,8]. γ Fe_2O_3 nanoparticles are ferrimagnetic in nature and exhibit spinel structure along with cation vacancies at octahedral sites. These vacancies along with competing surface interactions can lead to surface spins disorder and spin glass behavior in γ Fe_2O_3 nanoparticles [9]. Fiorani et al. [10] studied the dynamical and static properties of γ Fe_2O_3 nanoparticles which are governed by surface effects and interparticle interactions. These effects also decrease overall magnetization of nanoparticles as compared to bulk. Herlitschke et al. [11] observed 44% less magnetization in γ Fe_2O_3 nanospheres and 58% less magnetization in γ Fe_2O_3 nanocubes than bulk, which is due to spin disorder as analyzed by using nuclear resonant scattering and polarized neutrons.

Maghemite (γ Fe_2O_3) nanoparticles are highly reactive which lead to non functionalized surface and easily lose their magnetic properties. Therefore, proper surface coating or developing effective protection is essential to minimize surface energy and to prepare stable nanoparticles for potential applications [12]. Coating not only stabilizes nanoparticles but can also leads to surface functionalization. Different approaches for coating have been used so far which include coating with polymer, biomolecules, surfactants, magnetic and non magnetic etc. Prado et al. [13] reported an enhancement in the magnetic anisotropy of γ Fe_2O_3

* Corresponding author.
E-mail address: kashif.nadeem@iiu.edu.pk (K. Nadeem).

nanoparticles via the surface coordination of molecular complexes. Azhdarzadeh et al. [14] prepared gold coated iron oxide nanoparticles which are useful for photo thermal therapy of colan cancer and mag netic resonance imaging.

In this article, we have studied the surface effects in core shell Cr_2O_3 coated γ Fe_2O_3 nanoparticles as prepared by microwave plasma tech nique. Selection of antiferromagnetic (AFM) Cr_2O_3 coating is due to its desirable properties such as high hardness, mechanical strength, che mical inertness and low friction coefficient [15]. These properties make Cr_2O_3 coating very useful in the field of corrosion protection, wear resistance and surface modification [16]. Sahan et al. [17] observed surface modification of spinel $LiMn_2O_4$ by Cr_2O_3 coating and reported enhanced electrochemical properties for potential application. This study showed that Cr_2O_3 coating can be used for surface modification. The AFM Cr_2O_3 coating can also provide exchange bias phenomena in these nanoparticles due to core shell interactions. Therefore, it is in teresting to study the effects of Cr_2O_3 coating on magnetic properties of γ Fe_2O_3 nanoparticles. In this article, we have studied the surface ef fects in these Cr_2O_3 coated γ Fe_2O_3 nanoparticles by using dc and ac magnetic measurements and the experimental results were analyzed by using theoretical models.

2. Experiment

Cr_2O_3 coated γ Fe_2O_3 core shell nanoparticles have been prepared by microwave plasma synthesis technique using a 2.45 GHz magnetron with 2 consecutively arranged plasma zones, as shown in Ref. [18]. Liquid $Fe(CO)_5$ has been used as the precursor for Fe_2O_3 formation with a feeding rate of 7,5 ml/h, and solid $Cr(CO)_6$ as the precursor for Cr_2O_3 formation. The respective amount of precursors was selected to yield a volume ratio $Fe_2O_3 \div Cr_2O_3$ equal $1 \div 1$. Methylmethacrylic acid was used for the organic coating, yielding a monolayer of PMMA on top of each particle. The PMMA coating was used just for protection of core shell nanoparticles. Microwave power was set to 1500 W, the Ar/20 vol % O_2 reaction gas flow was adjusted to 10 L/min, yielding a system pressure of 10 mbar. The γ Fe_2O_3 cores are formed in the first plasma zone, acting as nuclei for the crystallization of the Cr_2O_3 shell in the second plasma zone. Polymer coating is performed immediately behind the second plasma zone. The principles of this synthesis process are reported elsewhere [19]. The resulting powder is dark brown. X ray diffraction (XRD) (Bruker D8 Advance instrument) was used for struc tural characterization by using Cu $K\alpha$ radiation at room temperature. Scanning Transmission Electron Microscopy (STEM) studies with re spect to nanoparticle size, morphology and core/shell structure were done on an aberration corrected Titan 80 300 Super Twin (FEI, Eind hoven, NL) instrument with field emission gun, operated at 300 kV, equipped with a GIF Tridium spectrometer with a BM UltraScan CCD camera (Gatan, Pleasantron, CA, USA). Standard TEM mode was used for imaging; STEM Electron Energy Loss Spectroscopy (EELS) maps with a frame size of 65 nm × 40 nm and a pixel size of 1 nm were ac quired with an energy dispersion of 0.3 eV/channel, including drift correction after 65 spectra respectively. The camera length was set to 0.038 m, and spot size 4 was used. The Cr L edge at 577 eV and the Fe L edge at 708 eV energy loss were evaluated using a Digital Micrograph® script [20]. Superconducting quantum interference device (SQUID) magnetometer (Quantum Design, MPMS XL 7) was used for ac and dc magnetic measurements.

3. Results and discussion

Powder X ray diffraction (XRD) is a characterization technique for identification of phases of crystalline material and determination of crystallite size. Fig. 1(a) shows the XRD pattern of Cr_2O_3 coated γ Fe_2O_3 nanoparticles. The broad peaks show the crystalline nature of γ Fe_2O_3 nanoparticles. The indexed peaks (220), (311), (400), (422), (511) and (440) at angles 30, 36, 43, 54, 57 and 63, respectively verify the inverse spinel structure of γ Fe_2O_3. While, the indexed peaks (012), (104), (110), (113), (024), (116), (214) and (1010) at angles 24, 33, 36, 41, 50, 54, 63 and 72, respectively correspond to the Cr_2O_3 phase [21,22]. High intensity diffracted peaks at angles 38, 44, 65 and 78 are from aluminum substrate. The diffracted peaks of Cr_2O_3 phase are narrower as compared to maghemite which implies the large crystallite size of Cr_2O_3 phase. The reason is the formation of Cr_2O_3 shell and also for mation of isolated Cr_2O_3 nanoparticles. The absence of impurity peaks in XRD scan confirms the high purity of the synthesized material. The average crystallite size of nanoparticles was calculated by using Debye Scherrer's formula,

$$D = \frac{k\lambda}{\beta \cos \theta} \tag{1}$$

where D is crystallite size, λ is the wavelength having constant value 0.1541 nm, β is the full width at half maxima, K is a shape constant and θ is the diffraction angle [23]. The average crystallite size of γ Fe_2O_3 nanoparticles is 13 nm. The intensive peaks of Cr_2O_3 in XRD indicate the higher concentration of Cr_2O_3 phase in the sample.

Transmission electron microscopy (TEM) is a powerful tool used for getting information about morphology of nanoparticles [24]. Fig. 1 (b) shows a TEM image of the nanoparticles at 10 nm scale. Most of the nanoparticles are spherical with moderate degree of agglomeration. Their size ranges from 5 to 20 nm. A core shell structure is hardly to detect in these nanoparticles, due to the weak difference in mass con trast of the phases Fe_2O_3 and Cr_2O_3, respectively. Fig. 1 (c) shows a STEM image. Also here, the contrast difference of the two phases of interest is very weak. The red marked area was analyzed by STEM EELS, and the results are shown in the insets. In detail, the insets show the color coded composition map (red: Fe, green: Cr), the detailed STEM image, and the STEM EELS images from the Cr L edge, the Fe L edge. Fig. 1 (d) shows the corresponding STEM EELS spectra from the core region and the shell region, marked by arrows. This analysis de monstrates that core shell nanoparticles are present. Nevertheless, the presence of bare Fe_2O_3 and bare Cr_2O_3 nanoparticles cannot be ex cluded.

Zero field cooled (ZFC) and field cooled (FC) protocols were used to study the temperature dependent magnetization of nanoparticles. Fig. 2 shows experimental (blue solid triangles) and simulated (red solid line) ZFC/FC dc susceptibility curves of Cr_2O_3 coated γ Fe_2O_3 nanoparticles at 50 Oe. For ZFC experimental curve, first sample is cooled from 300 to 4.2 K in zero field. Afterward, 50 Oe field is applied and magnetization is recorded by increasing temperature. For FC experimental curve, the sample is cooled down from 300 to 4.2 K with same 50 Oe field and magnetization is recorded on decreasing temperature [12]. The ZFC curve reveals maximum magnetization at 75 K which is average blocking temperature (T_B) of the nanoparticles. Just below the T_B, ex perimental FC curve turns out to be flat because magnetic moments of nanoparticles get frozen randomly and could not aligned themselves in a direction of applied magnetic field which is the clue for presence of interparticle interactions and/or surface spin disorder of Cr spins in these nanoparticles [4].

To get information of structural parameter and intrinsic magnetic properties of nanoparticles, ZFC/FC curves are simulated according to the model of non interacting particles. For simulation, we have used Neel Brown expression for relaxation time (τ_0) assuming uniaxial ani sotropy [25,26]. The temperature at which $\tau_0 = \tau_m$ (where τ_m is mea suring time) for a system of particles with average volume V, is known as blocking temperature T_B. Log normal distribution function for T_B is extracted from log normal distribution function for particle size and given as,

$$f(T_B)dT_B = \frac{1}{\sqrt{2\pi\sigma_{T_B}^2}} \frac{1}{T_B} \exp\left(\frac{In^2 \frac{T_B}{\langle T_B \rangle}}{2\sigma_{T_B}^2} \right) dT_B \tag{2}$$

Where σ_{T_B} is the "width" of the distribution of T_B which is a fixed

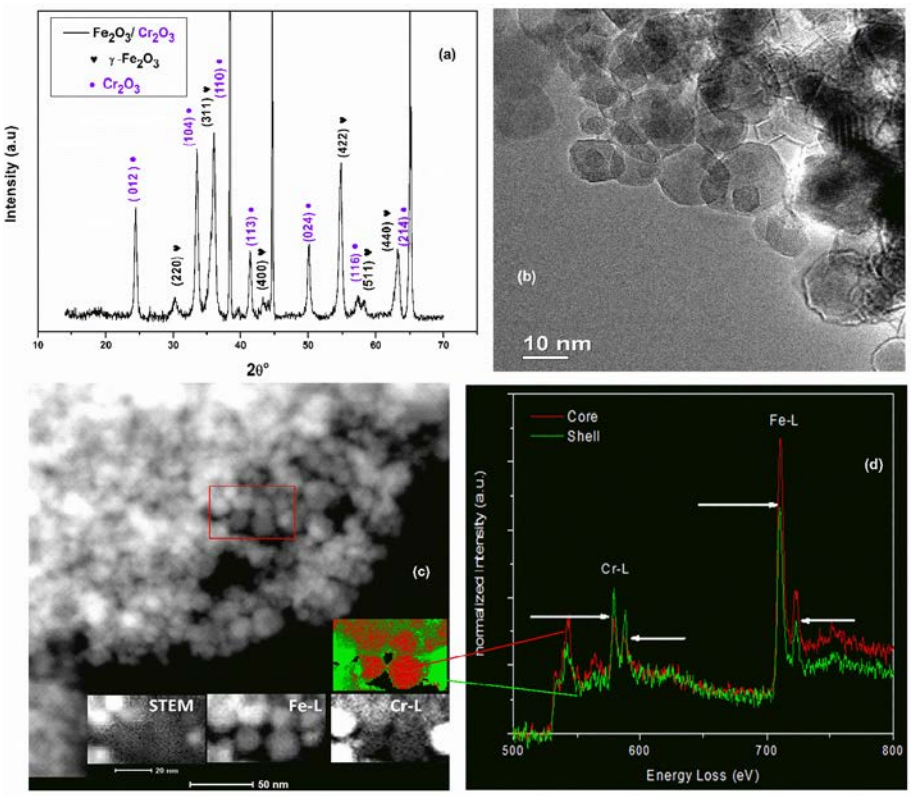

Fig. 1. (a) XRD pattern, **(b)** TEM image at 10 nm scale **(c)** STEM-image at 50 nm scale (inset shows the results of red marked area by STEM-EELS) of Cr_2O_3 coated γ-Fe_2O_3 nanoparticles and **(d)** STEM-EELS spectra of γ-Fe_2O_3 core (red color)-Cr_2O_3 shell (green color) nanoparticles. (For interpretation of the references to colour in this figure legend, the reader is referred to the web version of this article.)

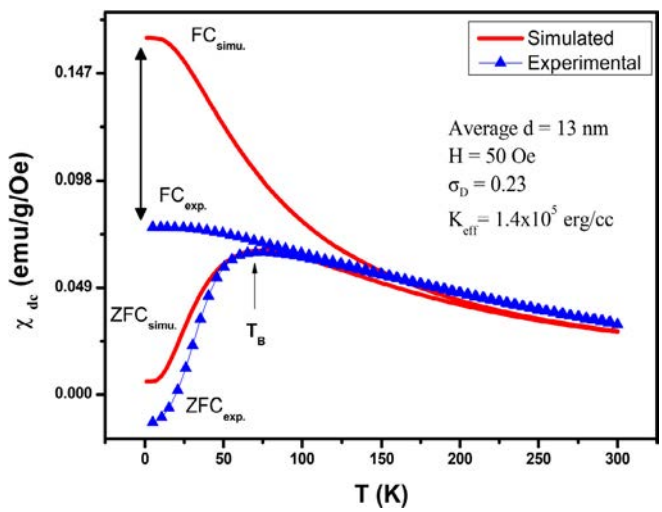

Fig. 2. ZFC/FC experimental (blue solid triangles) and simulated (red solid line) dc susceptibility curves of Cr_2O_3 coated γ-Fe_2O_3 nanoparticles under 50 Oe. (For interpretation of the references to colour in this figure legend, the reader is referred to the web version of this article.)

parameter of the chosen log norm function and $\sigma_{T_B} = \sigma_V = 3\,\sigma_D$. Since, average T_B is related to average volume V and given as,

$$\langle T_B \rangle = \frac{K_{eff}}{k_B In\frac{\tau_m}{\tau_0}} \langle V \rangle \tag{3}$$

Where K_{eff} is effective anisotropic constant and τ_o is atomic precession time. The ZFC dc susceptibility according to the model of non interacting particles consists of two contributions (i) and (ii) given as [27],

$$x_{ZFC}(T) = \frac{M_S^2}{3K}\left(\underbrace{In\left(\frac{\tau_m}{\tau_0}\right)\int_{TB=0}^{TB=T}\frac{T_B}{T}f(T_B)dT_B}_{(i)} + \underbrace{\int_{TB=T}^{TB=\infty} f(T_B)dT_B}_{(ii)}\right) \tag{4}$$

Where contribution (i) is due to superparamagnetic particles and contribution (ii) is for blocked particles. According to the same model, the FC dc susceptibility is [27],

$$x_{FC}(T) = \frac{M_S^2}{3K}In\left(\frac{\tau_m}{\tau_0}\right)\left(\underbrace{\left(\frac{1}{T}\right)\int_{TB=0}^{TB=T} T_B f(T_B)dT_B}_{(i)} + \underbrace{\int_{TB=T}^{TB=\infty} f(T_B)dT_B}_{(ii)}\right) \tag{5}$$

Using Eq. (4) and (5), we have fitted ZFC/FC susceptibility curve with $K_{eff} = 1.4 \times 10^5$ erg/cc and average particle size is 13 nm. The value of fitted K_{eff} is greater than bulk γ Fe_2O_3 (4.7×10^4 erg/cc) which is due to additional surface anisotropy offered by frozen disordered surface spins of Cr [10]. The K_{eff} of Cr_2O_3 coated γ Fe_2O_3 nanoparticles is less than bare γ Fe_2O_3 nanoparticles prepared by the same method (9.8×10^5 erg/cc) [28], which is due to relatively big particle size of coated nanoparticles. Moreover, big particle size with AFM surface layer may produce small value of interface anisotropy in core shell nanoparticles which results in decrease of fitted K_{eff}. Simulated curves also infer about moderate particle size distribution ($\sigma_D = 0.23$). A difference occurs between experimental and simulated FC curves at low temperatures. This is because real nanoparticles system contains interparticle interactions while model considers only non interacting nanoparticles. FC simulated curve does not flat immediately just below the T_B and flattens at very low temperature.

Fig. 3 (a) shows ZFC M H loop of Cr_2O_3 coated γ Fe_2O_3 nanoparticles at temperature 5 K under field of ± 5 T. The inset reveals expanded region of coercivity. The measured value of coercivity (H_C) and saturation magnetization (M_S) is 214 Oe and 19.7 emu/g, respectively which are nearly equal to reported value of H_C and M_S by Tzitzios et al.

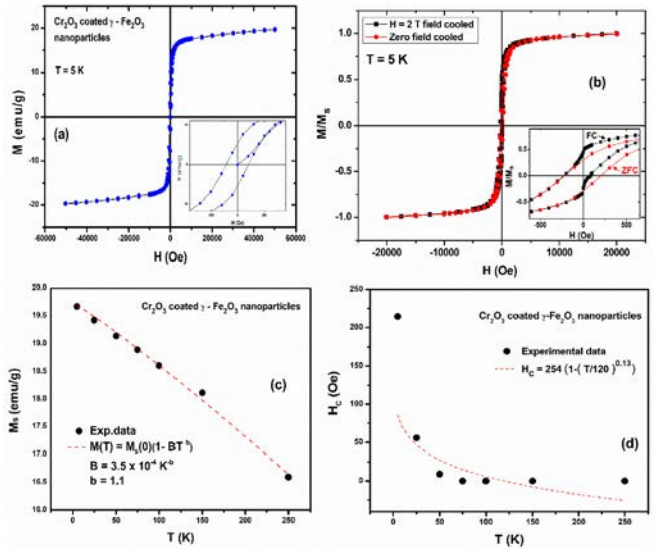

Fig. 3. (a) M-H loop at 5 K, (b) ZFC and FC (@ 2 T) M-H loops at 5 K, (c) M_S at different temperatures (dashed line shows the Bloch's law fit) and (d) H_C at different temperatures for Cr_2O_3 coated γ-Fe_2O_3 nanoparticles (dashed line shows the Kneller's law fit).

[29] of same sized γ Fe_2O_3 nanoparticles embedded in a laponite synthesized via one step chemical route. The magnetization appears to be the linear in the range 12 50 kOe. This linear trend is probably due to AFM Cr_2O_3 component and/or prominent disordered surface spins which causes the non saturation of M H loops. By subtracting this linear part, M_s value reduces to 17 emu/g. The measured M_S value is lower than bulk γ Fe_2O_3 (M_S = 80 emu/g) which is attributed to dangling and broken bonds at the nanoparticle's surface. At nanoscale, the dangling and broken bonds produce less coordination neighbors at surface which are responsible for decrease in exchange interactions and as a result M_S decreases in ferrite nanoparticles [10]. The M_S value of these Cr_2O_3 coated γ Fe_2O_3 nanoparticles is also much lower than bare γ Fe_2O_3 nanoparticles (prepared by the same method) M_S = 51 emu/g at same temperature [28], which is attributed to the presence of AFM wt.% of Cr_2O_3 phase in the normalization of magnetization in units of emu/g, frozen disordered surface spins of Cr. The observed value of H_C is low due to soft magnetic nature of γ Fe_2O_3 nanoparticles [30]. The H_C of Cr_2O_3 coated γ Fe_2O_3 nanoparticles is less than bare γ Fe_2O_3 nanoparticles (H_C = 546 Oe) [28]. The possible reason is bigger particle size of coated nanoparticles. The average crystallite size of Cr_2O_3 coated γ Fe_2O_3 nanoparticles (13 nm) produced with high feeding rate during synthesis than the uncoated γ Fe_2O_3 nanoparticles size (6 nm) as reported in Ref. [28]. The large coated nanoparticles have weak interface anisotropy between γ Fe_2O_3 ferrimagnetic core and Cr_2O_3 AFM shell which refers to lower effective anisotropy of coated nanoparticles than bare nanoparticles. Thus, AFM Cr_2O_3 shell and interfacial interactions play critical role in controlling the magnetization of γ Fe_2O_3 nanoparticles. Size dependent H_C is remarkable and Trohidou et al. [31] observed the same phenomena in Monte Carlo studies of ferromagnetic core and AFM shell nanocomposites.

Core shell nanoparticles exhibit an important phenomenon in which M H loop is shifted along the field axis using FC protocol is known as exchange bias effect. To confirm the exchange bias effect, we have taken FC M H loop and compared it with M H loop taken after ZFC. Fig. 3 (b) shows ZFC and FC (@ 2 T) M H loops of Cr_2O_3 coated γ Fe_2O_3 nanoparticles at 5 K. The inset reveals expanded region of coercivity. The FC loop is shifted only along the +ive field axis and also along the magnetization axis which confirmed the exchange bias effect in these nanoparticles [32]. This shifting of the loop is attributed to exchange bias effects caused by the FiM AFM core shell interactions [33].

We have also studied the temperature dependent M_S and H_C for our nanoparticles. We have taken partial ZFC M H loops of Cr_2O_3 coated γ Fe_2O_3 nanoparticles at temperatures T = 5, 25, 50, 100, 150 and 250 K under applied field of ± 5 T. Fig. 3(c) shows variation of M_S with temperature (solid spheres) and fitting of Bloch's law (red dashed line). Increasing trend of M_S with decreasing temperature is due to decreasing thermal fluctuations [34] which is according to prediction of Bloch's law. The equation for Bloch's law is,

$$M_S(T) = M_S(0)(1 - BT^b) \tag{6}$$

Where M_S (T) is a measured temperature dependent magnetization, M_S (0) is an extrapolated magnetization at 0 K, b and B are Bloch's exponent and Bloch's constant respectively which are used as fitting parameters. The value of B strongly depends on structure of materials and closely relates to exchange integral J as (B 1/J) [35]. Bloch's law is valid for bulk ferromagnetic materials with b = 3/2 but for nanomaterials, the value of b changes due to surface spins disorder, finite size effects and inter particles interactions [36]. We have fitted Bloch's law on our experimental M_S data, which provides the value of $B = 3.523 \times 10^{-4}\,K^{-b}$ and b = 1.10. The higher value of B than the bulk γ Fe_2O_3 is due to decreased particle size which results in weak exchange coupling J (B 1/J) arises from disorder at nanoparticle's surface. Lower value of b is due to no spin wave excitation at low temperatures in presence of large energy band gap at nano scale due to finite size effects [37]. Fig. 3(d) shows the variation of H_C (solid spheres) with temperature for the Cr_2O_3 coated γ Fe_2O_3 nanoparticles. H_C shows increasing trend with decreasing temperature which is due to decreasing thermal fluctuations and increased effective anisotropy at low temperatures [30]. H_C shows a sharp increase below 25 K due to disordered surface spins and FiM AFM core shell interactions, both contribute to effective anisotropy [4]. Molina et al. [38] also reported the sharp increase in H_C for $(Fe_{0.69}Co_{0.31})B_{0.4}$ nanoparticles which was attributed to increase in effective anisotropy at low temperatures. The temperature dependent H_C data can be fitted using Kneller's law valid for non interacting single domain nanoparticles as given in Eq. (7),

$$H_C(T)H_C(0)\left(1 - \left(\frac{T}{T_B}\right)^a\right) \tag{7}$$

Where H_C (0) is an extrapolated coercivity at 0 K, T_B is the average blocking temperature and α is constant having value 0.5 for bulk ferromagnetic material. Values of T_B and α got from the fit. Fig. 3(d) shows Kneller's law fit (red dashed line) on experimental H_C data for the Cr_2O_3 coated γ Fe_2O_3 nanoparticles with fitting parameters T_B = 120 K and α = 0.13 [39]. The fit is quite poor in entire temperature range. The deviation from the fit at low temperatures is due to sharp increase of H_C at low temperatures arises from the contribution of surface and core shell anisotropy below 25 K, which are not considered in Kneller's law. The deviation at high temperatures is due to superparamagnetic behavior [40,41]. The obtained value of T_B from Hc vs T data (120 K) is higher than the T_B = 75 K obtained from χ_{dc} vs T which is due to improper fit of Kneller's law.

DC magnetic measurements of Cr_2O_3 coated γ Fe_2O_3 nanoparticles signify the presence of surface spins disorder at low temperatures which can also cause spin glass behavior in these nanoparticles. A system having random alignment of magnetic spins with frustrated magnetic interactions is known as spin glass system. In spin glass temperature regime, the peak temperature also is known as cusp in the ac susceptibility usually shows variation with frequency. To study the spin glass behavior, we have measured frequency dependent ac susceptibility in the temperature range 5 300 K. Fig. 4 (a) depicts the frequency dependent in phase ac susceptibility of Cr_2O_3 coated γ Fe_2O_3 nanoparticles in frequency range from 1 to 1000 Hz under the ac field amplitude H_{ac} = 5 Oe. The curves show increasing trend of T_B (95 115 K) with increasing frequency (1 1000 Hz). This f shift of T_B can be analyzed through various laws such as Arrhenius law, Vogel Fulcher law

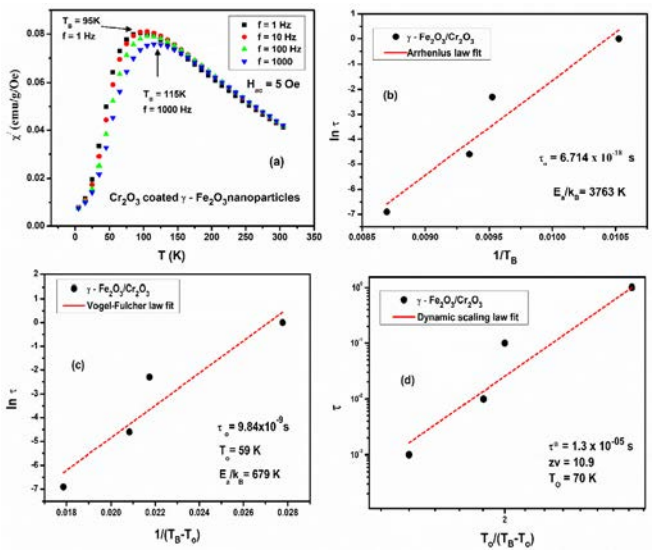

Fig. 4. (a) Temperature dependence of in-phase ac susceptibility for Cr_2O_3 coated γ-Fe_2O_3 nanoparticles. The frequency dependence of blocking temperature (T_B) is fitted with (b) Arrhenius law (c) Vogel-Fulcher law and (d) dynamic scaling law.

and dynamic scaling law. These laws are useful for getting information about interparticle interactions and spin glass behavior. Arrhenius law or Neel Brown relaxation model is valid for single domain non interacting particles [42]. This law is given as,

$$\tau = \tau_0 e\left(\frac{E_a}{k_B T_B}\right) \tag{8}$$

Where τ_o is the atomic spin flip time (10^{-9} to 10^{-12} s), E_a is the activation energy $E_a = K_{eff}V$ (K_{eff} is effective constant and V is the volume of particle) and k_B is the Boltzmann constant [43]. Fig. 4 (b) shows Arrhenius law fit on frequency dependent ac susceptibility for the Cr_2O_3 coated γ Fe_2O_3 nanoparticles. The fitted graph is a straight line between lnτ and $1/T_B$. In this fit, τ_o and E_a/k_B are used as fitting parameters and their values are $\tau_o = 6.71 \times 10^{-18}$ s and $E_a/k_B = 3763$ K. A very small value of τ_o and high value of E_a/k_B for these nanoparticles are unphysical. With these inadequate fitting parameters, Arrhenius law failed to analyze our system which also indicates the presence of interparticle interactions. To find out the interparticle interactions strength, we have used Vogel Fulcher law [44] having formula,

$$\tau = \tau_0 e\left(\frac{E_a}{k_B(T_B - T_o)}\right) \tag{9}$$

Where an additional parameter T_o represents the strength of interparticle interactions [45,46]. Fig. 4 (c) shows the Vogel Fulcher law fit for Cr_2O_3 coated γ Fe_2O_3 nanoparticles. The graph is a straight line between lnτ and $1/(T_B\ T_o)$ with fitting parameters $\tau_o = 9.84 \times 10^{-9}$ s, $E_a/k_B = 679$ K and $T_o = 59$ K. Now, both τ_o and E_a/k_B have reasonable values with high value of T_o which confirms the interparticle interactions among these nanoparticles. Dynamic scaling law is used to investigate the spin glass behavior and given as [28],

$$\tau = \tau^*\left(\frac{T_o}{T_B - T_0}\right)^{zv} \tag{10}$$

Where τ^* is the coherence time for coupled individual spins of nanoparticle, T_B is the frequency dependent freezing temperature (peak value of χ' T curve), T_o is the freezing temperature close to blocking temperature taken as fixed parameter and zv is a critical exponent. Value of zv lies between 4 and 12 for different typical spin glass systems. Fig. 4 (d) shows a dynamic scaling law fit for Cr_2O_3 coated γ Fe_2O_3 nanoparticles with fitting parameters $\tau^* = 1.3 \times 10^{-5}$ s and zv = 10.9. The value of zv lies within the range 4 12, which signify the spin glass behavior in these nanoparticles. High value of τ^* is due to frozen surface spins which increases the relaxation time of huge core spin of the nanoparticle [47,48]. The possible reason of spin glass behavior is disordered frustrated surface spins and random interparticle interactions.

4. Conclusions

We have studied the magnetic properties of Cr_2O_3 coated γ Fe_2O_3 nanoparticles prepared by microwave plasma synthesis technique. XRD analysis confirmed the inverse spinel structure of γ Fe_2O_3 nanoparticles. Average crystallite size of the nanoparticles was 13 nm. The ZFC/FC measurements revealed average blocking temperature of the nanoparticles at 75 K. Simulated ZFC/FC data exhibited the lower value of effective anisotropy constant of Cr_2O_3 coated γ Fe_2O_3 nanoparticles as compared to bare γ Fe_2O_3 nanoparticles which is due to relatively big particle size of coated nanoparticles and weak interface anisotropy between FiM core and AFM shell. Saturation magnetization showed an increasing trend with decreasing temperature and fitted with Bloch's law. Fitting showed higher value of Bloch's constant B than in bulk due to weaker exchange coupling on the surface of nanoparticle. The lower value of b is due to no spin wave excitation in presence of large energy band gap at nanoscale. The sharp increase of H_C at low temperatures is similar to bare nanoparticles and is attributed to enhanced surface disorder and core shell interactions. Nanoparticles also showed exchange bias effect which is attributed to FiM AFM core shell interactions. Arrhenius law is not fitted well to ac susceptibility data and revealed unphysical values of spin flip time and activation energy. Vogel Fulcher law fit provides reasonable values of spin flip time and activation energy with interaction parameter $T_o = 59$ K which ensures the presence of interparticle interactions. Dynamic scaling law fit confirmed the existence of spin glass behavior which is caused by the disordered surface spins and interparticle interactions. In conclusion, Cr_2O_3 coated γ Fe_2O_3 nanoparticles revealed Bloch's law fit with different parameters from bulk, deviation from Kneller's law, exchange bias effect and spin glass behavior, which are probably due to core shell interface interactions, interparticle interactions and surface disorder.

Acknowledgment

Authors acknowledge Higher Education Commission, Pakistan for financial support. Authors also acknowledge International Islamic University for providing research funds under project no. IIUI/ORIC/RP/HRSC/2016 518.

References

[1] M. Ushakov, M. Oshtrakh, I. Felner, A. Semenova, D. Kellerman, V. Šepelák, V. Semionkin, P. Morais, Magnetic properties of iron oxide-based nanoparticles: study using mössbauer spectroscopy with a high velocity resolution and magnetization measurements, J. Magn. Magn Mater. 431 (2017) 46–48.

[2] R.H. Kodama, A.E. Berkowitz, Atomic-scale magnetic modeling of oxide nanoparticles, Phys. Rev. B 59 (1999) 6321.

[3] A. Berkowitz, K. Takano, Exchange anisotropy—a review, J. Magn. Magn Mater. 200 (1999) 552–570.

[4] B. Martinez, X. Obradors, L. Balcells, A. Rouanet, C. Monty, Low temperature surface spin-glass transition in γ-Fe_2O_3 nanoparticles, Phys. Rev. Lett. 80 (1998) 181.

[5] R.H. Kodama, A.E. Berkowitz, E. McNiff Jr., S. Foner, Surface spin disorder in $NiFe_2O_4$ nanoparticles, Phys. Rev. Lett. 77 (1996) 394.

[6] E. Tronc, A. Ezzir, R. Cherkaoui, C. Chanéac, M. Nogues, H. Kachkachi, D. Fiorani, A. Testa, J. Greneche, J. Jolivet, Surface-related properties of γ-Fe_2O_3 nanoparticles, J. Magn. Magn Mater. 221 (2000) 63–79.

[7] C. Letti, L. Paterno, M. Pereira-da-Silva, P. Morais, M. Soler, The role of polymer films on the oxidation of magnetite nanoparticles, J. Solid State Chem. 246 (2017) 57–64.

[8] G.S. An, S.W. Choi, D.H. Chae, H.S. Lee, H.-J. Kim, Y. Kim, Y.-G. Jung, S.-C. Choi, γ-Fe_2O_3@SiO_2 core-shell structured nanoparticle: fabrication via surface treatment and application for plasmid DNA purification, Ceram. Int. 43 (2017) 12888–12892.

[9] K. Brymora, F. Calvayrac, Surface anisotropy of iron oxide nanoparticles and slabs from first principles: influence of coatings and ligands as a test of the heisenberg

model, J. Magn. Magn Mater. 434 (2017) 14–22.
[10] D. Fiorani, A. Testa, F. Lucari, F. D'Orazio, H. Romero, Magnetic properties of maghemite nanoparticle systems: surface anisotropy and interparticle interaction effects, Phys. B Condens. Matter 320 (2002) 122–126.
[11] M. Herlitschke, S. Disch, I. Sergueev, K. Schlage, E. Wetterskog, L. Bergström, R.P. Hermann, Spin disorder in maghemite nanoparticles investigated using polarized neutrons and nuclear resonant scattering, J. Phys. Conf. Ser., IOP Publishing (2016) 012002.
[12] F. Zeb, K. Nadeem, S.K.A. Shah, M. Kamran, I.H. Gul, L. Ali, Surface spins disorder in uncoated and SiO_2 coated maghemite nanoparticles, J. Magn. Magn Mater. 429 (2017) 270–275.
[13] Y. Prado, N. Daffé, A. Michel, T. Georgelin, N. Yaacoub, J.-M. Greneche, F. Choueikani, E. Otero, P. Ohresser, M.-A. Arrio, Enhancing the magnetic anisotropy of maghemite nanoparticles via the surface coordination of molecular complexes, Nat. Commun. 6 (2015) 10139.
[14] M. Azhdarzadeh, F. Atyabi, A.A. Saei, B.S. Varnamkhasti, Y. Omidi, M. Fateh, M. Ghavami, S. Shanehsazzadeh, R. Dinarvand, Theranostic Muc-1 aptamer targeted gold coated superparamagnetic iron oxide nanoparticles for magnetic resonance imaging and photothermal therapy of colon cancer, Colloids Surfaces B Biointerfaces 143 (2016) 224–232.
[15] K. Girisha, K.S. Rao, K. Anil, S. Sanman, Experimental investigation on erosive wear behaviour of plasma spray coated stainless steel, IOP Conf. Ser.: Mater. Sci. and Engin., IOP Publishing (2017) 012022.
[16] N. He, H. Li, L. Ji, X. Liu, H. Zhou, J. Chen, Reusable chromium oxide coating with lubricating behavior from 25 to 1000° C due to a self-assembled mesh-like surface structure, Surf. Coating. Technol. 321 (2017) 300–308.
[17] H. Şahan, H. Göktepe, Ş. Patat, A. Ülgen, Effect of the Cr_2O_3 coating on electrochemical properties of spinel $LiMn_2O_4$ as a cathode material for lithium battery applications, Solid State Ionics 181 (2010) 1437–1444.
[18] D.V. Szabó, S. Schlabach, Microwave plasma synthesis of materials—from physics and chemistry to nanoparticles: a materials Scientist's viewpoint, Inorganics 2 (2014) 468–507.
[19] D. Vollath, D.V. Szabó, The microwave plasma process–a versatile process to synthesise nanoparticulate materials, J. Nanoparticle Res. 8 (2006) 417–428.
[20] D. Mitchell, B. Schaffer, Scripting-customised microscopy tools for digital Micrograph™, Ultramicroscopy 103 (2005) 319–332.
[21] S. Rajput, L.P. Singh, C.U. Pittman, D. Mohan, Lead (Pb^{2+}) and copper (Cu^{2+}) remediation from water using superparamagnetic maghemite (γ-Fe_2O_3) nanoparticles synthesized by flame spray pyrolysis (fsp), J. Colloid Interface Sci. 492 (2017) 176–190.
[22] K. Mohanapandiana, A. Krishnanb, Synthesis, structural, morphological and optical properties of Cu^{2+} doped Cr_2O_3 nanoparticles, Int. J. Adv. Eng. Technol. 273 (2016) 279.
[23] M. Kamran, A. Ullah, Y. Mehmood, K. Nadeem, H. Krenn, Role of SiO_2 coating in multiferroic $CoCr_2O_4$ nanoparticles, AIP Adv. 7 (2017) 025011.
[24] M. Kamran, A. Ullah, S. Rahman, A. Tahir, K. Nadeem, M.A. ur Rehman, S. Hussain, Structural, magnetic, and dielectric properties of multiferroic $Co_{1-x}Mg_xCr_2O_4$ nanoparticles, J. Magn. Magn Mater. 433 (2017) 178–186.
[25] L. Néel, Theory of magnetic scrambling of diffusion, J. Phys. Radium 13 (1952) 249–264.
[26] W.F. Brown Jr., Thermal fluctuations of a single-domain particle, Phys. Rev. 130 (1963) 1677.
[27] J.C. Denardin, A. Brandl, M. Knobel, P. Panissod, A. Pakhomov, H. Liu, X. Zhang, Thermoremanence and zero-field-cooled/field-cooled magnetization study of $co_x(SiO_2)_{1-x}$ granular films, Phys. Rev. B 65 (2002) 064422.
[28] K. Nadeem, H. Krenn, T. Traussnig, R. Würschum, D. Szabó, I. Letofsky-Papst, Spin-glass freezing of maghemite nanoparticles prepared by microwave plasma synthesis, J. Appl. Phys. 111 (2012) 113911.
[29] V. Tzitzios, G. Basina, A. Bakandritsos, C.G. Hadjipanayis, H. Mao, D. Niarchos, G.C. Hadjipanayis, J. Tucek, R. Zboril, Immobilization of magnetic iron oxide nanoparticles on laponite discs–an easy way to biocompatible ferrofluids and ferrogels, J. Mater. Chem. 20 (2010) 5418–5428.
[30] J. Smit, H.P.J. Wijn, Ferrites: Physical Properties of Ferrimagnetic Oxides in Relation to Their Technical Applications, Wiley, 1959.
[31] K. Trohidou, Monte Carlo Studies of Surface and Interface Effects in Magnetic Nanoparticles, Surface Effects in Magnetic Nanoparticles, (2005), pp. 45–74.
[32] S. Ye, T. Nozaki, Y. Kotani, K. Toyoki, T. Nakamura, S. Yonemura, T. Shibata, S.P. Pati, M. Al-Mahdawi, Y. Shiokawa, Inserted metals for low-energy magnetoelectric switching in a Cr_2O_3/Ferromagnet interfacial exchange-biased thin film system, J. Mater. Chem. C 6 (2018) 2962–2969.
[33] I. Schmid, The Role of Uncompensated Spins in Exchange Biased Systems, in, University of Basel, 2008.
[34] M.U. Rahman, M. Usman, S.K. Hasanain, A. Ullah, I.W. Kim, Static magnetic properties of maghemite nanoparticles, J. Kor. Phys. Soc. 65 (2014) 1925–1929.
[35] R. Aragón, Magnetization and exchange in nonstoichiometric magnetite, Phys. Rev. B 46 (1992) 5328.
[36] D.T.T. Nguyet, N.P. Duong, L.T. Hung, T.D. Hien, T. Satoh, Crystallization and magnetic behavior of nanosized nickel ferrite prepared by citrate precursor method, J. Alloy. Comp. 509 (2011) 6621–6625.
[37] D. Zhang, K. Klabunde, C. Sorensen, G. Hadjipanayis, Magnetization temperature dependence in iron nanoparticles, Phys. Rev. B 58 (1998) 14167.
[38] B. Molina-Concha, R.D. Zysler, H. Romero, Anomalous magnetization enhancement and frustration in the internal magnetic order on $(Fe_{0.69}Co_{0.31})B_{0.4}$ nanoparticles, Appl. Sci. 2 (2012) 315–326.
[39] K. Maaz, S. Karim, K.J. Lee, M.-H. Jung, G.-H. Kim, Effect of temperature on the magnetic characteristics of $Ni_{0.5}Co_{0.5}Fe_2O_4$ nanoparticles, Mater. Chem. Phys. 133 (2012) 1006–1010.
[40] S. Chen, P. Andre, Colloidal syntheses of FePt nanoparticles, Int. J. Nanotechnol. 9 (2012) 39–68.
[41] C. Chinnasamy, A. Narayanasamy, N. Ponpandian, R.J. Joseyphus, B. Jeyadevan, K. Tohji, K. Chattopadhyay, Grain size effect on the néel temperature and magnetic properties of nanocrystalline $NiFe_2O_4$ spinel, J. Magn. Magn Mater. 238 (2002) 281–287.
[42] V. Singh, M. Seehra, J. Bonevich, Ac susceptibility studies of magnetic relaxation in nanoparticles of Ni dispersed in silica, J. Appl. Phys. 105 (2009) 07B518.
[43] D. Kim, Y. Zhang, W. Voit, K. Rao, M. Muhammed, Synthesis and characterization of surfactant-coated superparamagnetic monodispersed iron oxide nanoparticles, J. Magn. Magn Mater. 225 (2001) 30–36.
[44] B. Aslibeiki, P. Kameli, H. Salamati, M. Eshraghi, T. Tahmasebi, Superspin glass state in $MnFe_2O_4$ nanoparticles, J. Magn. Magn Mater. 322 (2010) 2929–2934.
[45] S. Shtrikman, E. Wohlfarth, The theory of the vogel-fulcher law of spin glasses, Phys. Lett. 85 (1981) 467–470.
[46] S. Mørup, Superparamagnetism, Spin Glass, Ordering in magnetic nanocomposites, Europhys. Lett. 28 (1994) 671.
[47] K. Fischer, J. Hertz, Spin-glasses, Volume 1 of Cambridge Studies in Magnetism, Cambridge university press, Cambridge, 1991.
[48] J. Mohapatra, A. Mitra, D. Bahadur, M. Aslam, Superspin glass behavior of self-interacting $CoFe_2O_4$ nanoparticles, J. Alloy. Comp. 628 (2015) 416–423.